Local-flux vectors of conserved quantities in wavenumber space: Anisotropic structures in Charney–Hasegawa–Mima turbulence

Masanori Takaoka [*]

Department of Mechanical Engineering and Science, Doshisha University, Kyotanabe 610-0394, Japan

Naoto Yokoyama

Department of Mechanical Engineering, Tokyo Denki University, Adachi 120-8551, Japan

Eiichi Sasaki

Department of Systems Design Engineering, Akita University, Akita 010-8502, Japan

Local-flux vectors of conserved quantities in the wavenumber space are proposed to investigate their directional properties in anisotropic turbulence. The proposed vectors are validated in statistically steady states of Charney-Hasegawa-Mima turbulence, which consists of anisotropic wave turbulence with zonal flow and isotropic vortex turbulence. The directions of the local-flux vectors are consistent with the energy-enstrophy double cascade in two-dimensional isotropic turbulence. The flux vectors of energy, furthermore, successfully show an anisotropic structure below the Rhines wavenumber, corresponding to the large-scale zonal flow, while those of enstrophy show almost isotropic structure. A couple of expressions of the critical balance are compared with the energy spectra and the flux vectors. The results confirm that the proposed method can quantitatively characterize the anisotropically directed flows of conserved quantities in the wavenumber space.

Simultaneous existence of more than one inviscid invariant is one of the most intriguing properties of two-dimensional (2D) fluid turbulence [1]. For three-dimensional (3D) homogeneous isotropic turbulence (HIT), the cascade theory initiated by Kolmogorov [2], which is based on Richardson's idea of cascading vortices from large to small scales, successfully reveals the statistical properties. Energy conservation results in the constant energy flux owing to the local equilibrium state within the inertial subrange of scales. For 2D HIT, Kraichnan has shown in his seminal work [3] that energy cascades to larger scales during counterintuitive turbulent self-organization, called inverse cascade, while enstrophy cascades to smaller scales. The idea of such double cascade was first suggested by Fjørtoft [4] based on the conservation of the two quadratic positive-definite invariants. The confirmation of the double cascade has been a longstanding source of controversy (see, e.g., Ref. [5] and references therein). The emergence of large coherent structures in 2D turbulence has become the subject of intense research recently by using high-resolution long-time simulations, for instance [6]. Extension of the cascade theory to anisotropic turbulence has been attempted and is still considered as an open problem (see Ref. [7] and references therein). The quantification of energy fluxes is eagerly anticipated to validate such extension and especially the idea of critical balance, which is supposed to have some universality [8,9].

[*]mtakaoka@mail.doshisha.ac.jp

Energy flux in the wavenumber space ($\boldsymbol{k}$ space) plays a pivotal role in elucidating turbulence properties. Although anisotropic turbulence is ubiquitously observed at least in large scales, little is known about its energy flux in contrast to the well-formulated cascade theory in HIT. One of the essential difficulties comes from the indefiniteness of the intermode transfers in nonlinear interaction as discussed in Ref. [10] and later in this Letter. Even recently, alternative expressions to uniquely determine intermode transfers have been actively proposed by decomposing the triad interaction of the nonlinear term [11]. In Ref. [12], the authors proposed the minimal-norm energy-flux vectors in anisotropic turbulence by employing the idea of least-action principle in the system where the Euclidean norm of the energy-flux vector is considered as an action. The energy flux in heterogeneous coexistence turbulence (HCT), where anisotropic wave turbulence and isotropic vortex turbulence coexist, is a major unresolved issue. We here propose more generalized practical formulation of the flux vectors and quantify fluxes in HCT including transition wavenumber range.

Inspired by Ref. [13], Charney–Hasegawa–Mima (CHM) turbulence, which describes the common physics in both the Rossby waves in the quasigeostrophic flow and the drift waves in a magnetically confined plasma, is adopted as a representative test field. The governing equation in the present direct numerical simulation (DNS) is written in $\boldsymbol{k}$ space as:

$$\frac{\partial \hat{\zeta}}{\partial t}(\boldsymbol{k}, t) = \sum_{\boldsymbol{k}=\boldsymbol{k}_1+\boldsymbol{k}_2} (\boldsymbol{k}_1 \times \boldsymbol{k}_2)_z \hat{\zeta}(\boldsymbol{k}_1, t)\hat{\psi}(\boldsymbol{k}_2, t) - ik_x\beta\hat{\psi}(\boldsymbol{k}, t) - \hat{D}(\boldsymbol{k}, t) + \hat{F}(\boldsymbol{k}, t), \qquad (1)$$

where $\hat{\zeta}$ and $\hat{\psi}$ are, respectively, the Fourier coefficients of the vorticity ζ and the stream function ψ, which have the relation $\hat{\zeta} = (k_x^2 + k_y^2)\hat{\psi}$, and $\hat{D}$ and $\hat{F}$ are, respectively, those of the dissipation D and the external forcing F, which are added to achieve statistically steady state.

The CHM equation has two quadratic invariants, energy $\int (1/2)(k_x^2 + k_y^2)|\hat{\psi}|^2 d\boldsymbol{k}$ and enstrophy $\int (1/2)|\hat{\zeta}|^2 d\boldsymbol{k}$, and shows rich turbulence states: zonal flows, and wave turbulence above the Rhines scale [14] and the 2D NS turbulence below it. In $\boldsymbol{k}$ space, they correspond to the dumbbell spectrum, will be seen in Fig. 4 later, in lower-wavenumber range [15], and the isotropic energy-enstrophy double cascade in higher-wavenumber range [3,4]. Although a predicted scenario of the energy flux based on the idea of the critical balance is illustrated in Ref. [9], such energy flux has never been quantitatively evaluated as far as the authors know.

Recently, Fjørtoft's argument is generalized to find the anisotropic directions of triple cascade including zonostrophy, which is a quadratic quasiconserved quantity [16], in the CHM turbulence [13]. The motions of centroids of these three (quasi)conserved quantities are employed to visualize the directions of the fluxes in developing turbulence. Although the idea of centroid is intuitive and acceptable, it works only for a localized spectrum in a developing state. We here take an alternative approach to quantify fluxes, which works both in developing and statistically steady states regardless of spectral distributions.

In isotropic systems, transfers of conserved quantities can be described as scalar functions of $k = |\boldsymbol{k}|$ and obtained by their spectrum equations derived from governing equations. The flux $P(k, t)$ of a conserved quantity $I(k, t)$ at time t through a constant-$|\boldsymbol{k}|$ circle (a sphere in three dimensions) is related to its transfer function via nonlinear interactions $T(k, t) = [\partial I(k, t)/\partial t]_{NL}$ as $T(k, t) + [\partial P(k, t)/\partial k] = 0$. The fluxes in anisotropic turbulence should be considered as a vector field to describe a flow in $\boldsymbol{k}$ space to have directional properties. Drawing fluxes as a vector field implicitly assumes the dominance of local interaction as a net transfer as in the cascade theory and diffusion models [17]. Cancellation of nonlocal interactions is reported in HIT [10]. Let us define a flux vector $\boldsymbol{P}(\boldsymbol{k}, t)$ of an invariant $I(\boldsymbol{k}, t)$ as the flow by using its transfer function $T(\boldsymbol{k}, t) = [\partial I(\boldsymbol{k}, t)/\partial t]_{NL}$ similarly to isotropic one. Since $I(\boldsymbol{k}, t)$ is conserved while flowing in $\boldsymbol{k}$ space, $\boldsymbol{P}(\boldsymbol{k}, t)$ satisfies a continuity equation:

$$T(\boldsymbol{k}, t) + \mathrm{div}_{\boldsymbol{k}}\boldsymbol{P}(\boldsymbol{k}, t) = 0, \qquad (2)$$

where $\mathrm{div}_{\boldsymbol{k}}$ is the divergence operator in $\boldsymbol{k}$ space. It is impossible to uniquely determine $\boldsymbol{P}(\boldsymbol{k}, t)$ only from this scalar equation (2), although reported is a singular exception of a weak-turbulence system
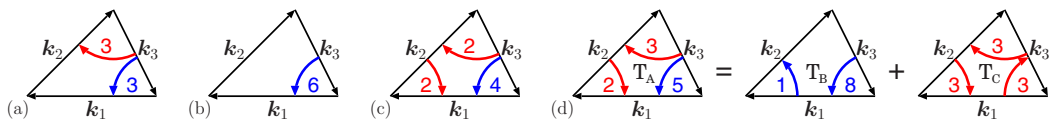
FIG. 1. Conceptual diagram of intermode transfers in triad interactions: (a) a symmetric-type example, (b), (c) catalytic-type examples, and (d) an example of circulation indefiniteness. Curved arrows represent intermode transfers.

where the dispersion law and the interaction coefficient in the kinetic equation are hypothetical bihomogeneous functions [18], which does not hold in general, especially in HCT. In the limit of weak nonlinearity, a kinetic equation for condensation, e.g., turbulence pileup and zonal flows, of turbulent spectrum at large scales predicts nonlocal interactions due to resonance in weak-turbulence theory [9,18,19]. However for HCT, the prediction based on a kinetic equation cannot be applied because of the strong nonlinearity. Moreover, for a statistically steady turbulence, which implies time scale is much longer than a resonance time scale, one may expect all modes are connected directly or indirectly [20].

Briefly reviewing the circulation indefiniteness of the intermode transfers, we propose an idea to uniquely determine $P(k, t)$. As known from Eq. (1), the intermode transfer of a quadratic invariant I, for example, is represented by the triad interaction among k_1, k_2, and k_3, satisfying $k_1 + k_2 + k_3 = 0$. A symmetric type is commonly acceptable example to uniquely determine the transfer: considering the case that both $I(k_1)$ and $I(k_2)$ obtain 3, while $I(k_3)$ loses 6, the intermode transfers are naturally determined as drawn in Fig. 1(a) owing to its symmetry. On the other hand, catalytic type of the interaction may evoke a variety of intermode transfers. Considering the case that $I(k_1)$ obtains 6, $I(k_2)$ does not change and $I(k_3)$ loses 6, one may simply draw as in Fig. 1(b). However, since k_2 plays a part of the triad and its obtained value 0 is the midvalue between the obtained values 6 and -6, another may draw as in Fig. 1(c). In Fig. 1(d), circulation indefiniteness is illustrated: consider the case that k_1, k_2, and k_3 obtain 7, 1, and -8, respectively. The intermode transfer T_A in Fig. 1(d) gives equivalent transfers with T_B, for example, owing to the indefiniteness of a circulation transfer T_C. We here introduce an ansatz that the intermode transfer is proportionate to the difference between the obtained value of the two modes, which uniquely determine the transfers as T_A in Fig. 1(d), i.e., $3 = [1 - (-8)]/3$, $2 = (7 - 1)/3$, and $5 = [7 - (-8)]/3$ where the proportionality factor is $1/n$ for n-mode interaction. Detailed balance leads that intermode transfers have no circulation, i.e., irrotational. For $P(k, t)$, the flux across a closed curve or a line (a closed surface or a plane in three dimensions) also has the indefiniteness of circulating flow. A conservative vector field, also called a path-independent vector field, may be the first candidate for removal of such indefiniteness. We here define $P(k, t)$ as a conservative vector that satisfies Eq. (2) and give the name of local-flux vector.

In Ref. [12], Eq. (2) for energy is evaluated using a coarse-grained finite difference approximation in k space, which yields a noninvertible matrix and vector problem for P. The minimal-norm energy-flux vectors was proposed by employing a special solution owing to the Moore-Penrose inverse. Since a conservative vector is irrotational and can be represented by a scalar potential, the local-flux vector proposed here can be obtained by the inverse Laplacian in k space instead of the Moore-Penrose inverse. The local-flux vector of energy should be the same as that in Ref. [12], because rotational flow belongs to the null space of the divergence operator in Eq. (2). As known from the derivation, the proposed vector is a natural generalization of conventional flux; by integrating over constant $|k|$ (or constant k_x, k_y and so on) it agrees with the conventional one.

HIT of 2D Navier–Stokes (NS) equation is adopted as a preliminary test because of the double cascade [3,4], although the energy and the enstrophy flow only in radial direction. The standard 2/3-dealiased spectral method was employed on 2048^2 grid points in the periodic square $[0, 2\pi]^2$. A fourth-order Runge–Kutta scheme with linear terms treated implicitly was used for time marching.
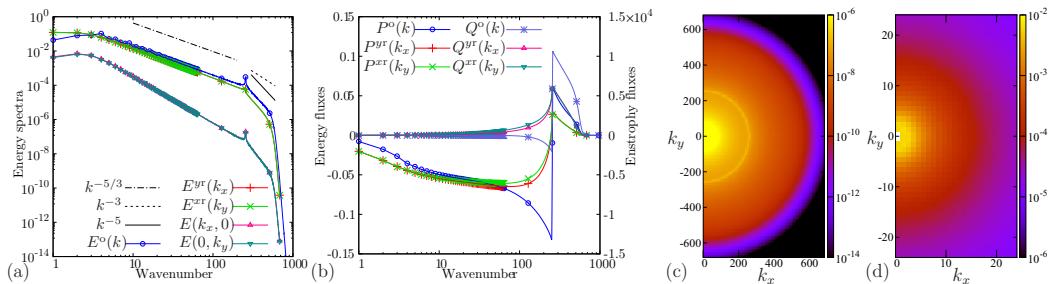
FIG. 2. In HIT, (a) energy spectra, where $E^o(k)$, $E^{yr}(k_x)$, $E^{xr}(k_y)$, $E(k_x, 0)$, and $E(0, k_y)$, respectively represent, omnidirectional, unidirectionally reduced, and on-axis energy spectra. (b) Fluxes of energy and enstrophy, which are defined similarly to omnidirectional and unidirectionally reduced spectra. The symbols are plotted at only representative wavenumbers in the high-wavenumber range. (c) 2D energy spectrum in the right half plane, and (d) its low-wavenumber enlargement, where they are colored in the logarithmic scale by adjusting the color range to show the structure clearly.

The high-wavenumber forcing, whose amplitude is set for the energy density to be of order unity, was added at $|\boldsymbol{k}| \approx 256 =: k_f$ to investigate the dumbbell spectrum in the inverse cascade. The hypodrag and hyperviscosity are set, respectively, as $\mu_m |\boldsymbol{k}|^{-2m}$ and $\nu |\boldsymbol{k}|^2 + \nu_n |\boldsymbol{k}|^{2n}$ [21]. We adopted the values of $m = 0.3$, $n = 8$, $\mu_m = 1.0 \times 10^{-1}$ and $\nu_n = 1.0 \times 10^{-42}$, and ν as $\nu k_s^2 = \nu_n k_s^{2n}$ at $k_s = 512$.

For HIT, conventional 1D spectra and fluxes are plotted in Figs. 2(a) and 2(b). The omnidirectional spectrum $E^o(k)$ was obtained by integrating over azimuthal direction with $|\boldsymbol{k}|$ fixed. Two other kinds of 1D spectra are introduced: the one, here called unidirectionally reduced spectrum, $E^{yr}(k_x)$ [$E^{xr}(k_y)$], is obtained by integrating over the other independent variable k_y (k_x), and the other, on-axis spectrum, $E(k_x, 0)$ [$E(0, k_y)$], is the spectrum on each axis. The fluxes of energy and enstrophy defined in the similar way to the spectra are plotted in Fig. 2(b): omnidirectional flux of energy $P^o(k)$ and enstrophy $Q^o(k)$, and unidirectionally reduced ones $P^{yr}(k_x)$ [$P^{xr}(k_y)$] and $Q^{yr}(k_x)$ [$Q^{xr}(k_y)$]. The unidirectionally reduced spectra, $E^{yr}(k_x)$ [$E^{xr}(k_y)$], and fluxes, $P^{yr}(k_x)$ etc., include all turbulence information in $|\boldsymbol{k}| > k_x$ (k_y). Comparison of $P^o(k)$ and $P^{yr}(k_x)$ [$P^{xr}(k_y)$] in the range of $50 \lesssim k \leqslant k_f$ in Fig. 2(b) provides an example for this fact, since the difference between the convex upward and downward comes from $|\boldsymbol{k}| > k_f$ especially where the flux has the opposite sign. Note that the Newtonian viscosity is also effective slightly below the forcing wavenumber. Although the periodic boundary condition does not meet invariance under arbitrary rotation for isotropy, it is not evident in these 1D spectra and fluxes. Therefore 2D spectra and local-flux vectors are indispensable to reveal this fact.

In Fig. 2(a), while the predicted power law of $k^{-5/3}$ can be seen in the inverse-cascade range, much steeper spectra than the enstrophy-cascade spectrum with k^{-3} are observed in the forward-cascade range. The double-cascade spectrum cannot be produced by band-limited forcing, and the slope of the forward-cascade energy spectra cannot be shallower than -5 [22]. While the constant energy flux is achieved approximately in the inverse-cascade range, the constant enstrophy flux is not in the forward-cascade range, as shown in Fig. 2(b). It also appears in a different way that the inverse cascade of enstrophy is negligible, while the forward cascade of energy is not. Although the latter range is too narrow to achieve pure enstrophy cascade, the energy flux should be smaller for wider forward-cascade range [23]. It is, however, sufficient for the present purpose that most of the energy and the enstrophy cascade in backward and forward directions, respectively. The 2D energy distribution in HIT has 2D axisymmetry as shown in Fig. 2(c) and its enlargement in low-wavenumber range in Fig. 2(d). They are shown only in the right half of (k_x, k_y) plane because of the conjugate symmetry of the Fourier coefficients.
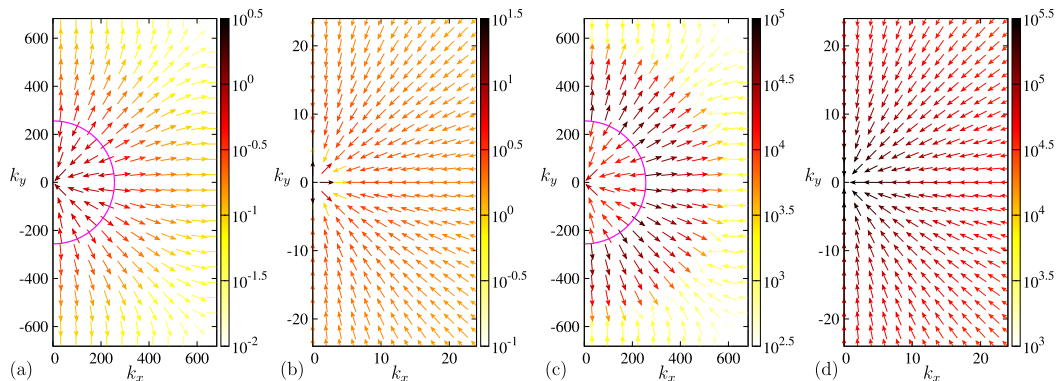
FIG. 3. In HIT, local-flux vectors of (a), (b) energy and (c), (d) enstrophy. See also the caption to Figs. 2(c) and 2(d). The vectors are shown by equal-length arrows to make their direction visible and colored to represent their magnitudes in logarithmic scale. The color range is adjusted to show the magnitudes clearly. The magenta semicircle represents forced wavenumbers.

Figures 3(a) and 3(b) display the local-flux vectors of energy in the region corresponding to Figs. 2(c) and 2(d), respectively. These vectors are shown at a periodic sampling of grid points to improve visibility, although they are determined at every grid points. The vectors point radially inward (outward) inside (outside) the semicircle of the forced wavenumbers as seen in Fig. 3(a). However, owing to the rectangular shape of outer boundary the directions of the vectors deviate from radial ones near the highest wavenumber where their magnitudes are negligibly small as noticed from their colors. Although there exist outward vectors in the lower-wavenumber range, where they are remarkably enhanced by k^{-1} factor due to arc length of the circle, they are very small as confirmed by Fig. 2(b). The sink on the semicircle $|\boldsymbol{k}| \approx 3$ is consistent with the existence of strong dissipation by the hypodrag as recognized from Fig. 2(d). The local-flux vectors of enstrophy are shown in Figs. 3(c) and 3(d). Although the flux vectors are directed as if the forcing region is a dividing ridge as observed in the energy-flux vectors, the enstrophy-flux vectors have large magnitude just outside the forcing wavenumber and precipitously drops beyond $|\boldsymbol{k}| \approx 400$ as seen in Fig. 3(c). Directional reversal and anisotropy around $|\boldsymbol{k}| \approx 450$ are, respectively, due to the artificially added hyperviscosity and the square boundary condition, and its magnitude is small to be neglected even in the integrated flux, as implied by the omnidirectional flux [Fig. 2(b)]. The appearance of large values around the origin in Fig. 3(d) is again due to the k^{-1} factor. These results show that the proposed flux vectors are consistent with the energy-enstrophy double-cascade scenario [3,4].

In the CHM turbulence, the inverse energy cascade would be altered and redirected toward zonal modes below a transition wavenumber between the ranges of isotropic turbulence and Rossby-wave turbulence [14]. Equating the magnitudes of the linear and nonlinear terms in Eq. (1), term balancing for brevity, one obtains the Rhines wavenumber $k_{\mathrm{R}} = \sqrt{\beta/U}$ [1]: equating the linear term $(\sim |\beta k_x \Psi|)$ and the nonlinear term $(\sim |k_x k_y Z \Psi|)$ leads $\beta \sim |k_y Z| = |k_y k^2 \Psi| \sim k^2 U$, where Ψ, Z, and U are, respectively, the characteristic values of $\hat{\psi}$, $\hat{\zeta}$, and the x component of the velocity $\hat{u} = i k_y \hat{\psi}$. On the other hand, balancing the linear and nonlinear time scales, time balancing, one also obtains the dumbbell spectrum: equating the Rossby wave period $k^2/(\beta|k_x|)$ as the linear time scale and the eddy turnover time $(\epsilon k^2)^{-1/3}$, owing to a Kolmogorov-type estimate, as the nonlinear time scale,

---

[1]Rhines originally obtained $k_{\mathrm{R}} = \sqrt{\beta/(2U)}$ by setting the orientation averaged phase speed of the Rossby wave as $\beta/(2k^2)$ with the assumption of a narrow spectrum.
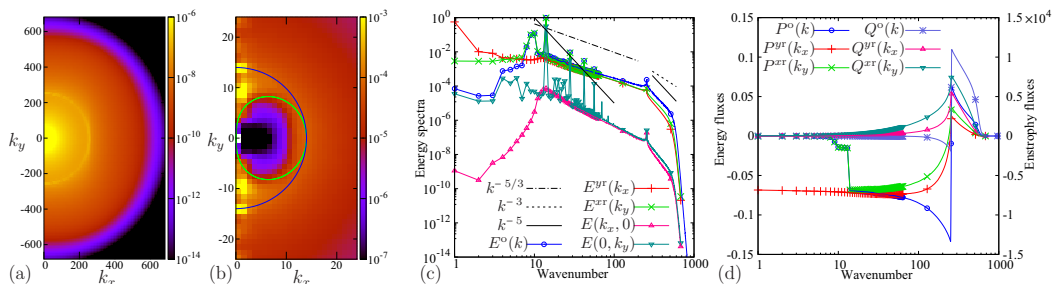
FIG. 4. In CHM turbulence, (a) 2D energy spectrum in the right half-plane, (b) its low-wavenumber enlargement, (c) energy spectra, and (d) fluxes of energy and enstrophy. The blue and green curves, respectively, represent $|\boldsymbol{k}| = k_{\rm R}^\star$ and $k^8 = (k_\beta^\star)^5|k_x|^3$ with $k_{\rm R}^\star = k_\beta^\star = 14$. See also the caption to Fig. 2.

leads $k^8 = k_\beta^5|k_x|^3$ where $k_\beta = (\beta^3/\epsilon)^{1/5}$ and ϵ is the energy transfer rate. Other nonlinear time scales yields other functional forms of dumbbell spectrum [15].

The 2D energy spectra of the CHM turbulence with $\beta = 10^3$, which leads $k_{\rm R} \approx 25$ and $k_\beta \approx 1.1 \times 10^2$, are drawn in Figs. 4(a) and 4(b) as in Figs. 2(c) and 2(d). While the 2D spectrum shows isotropy in the higher-wavenumber range [Fig. 4(a)], the dumbbell spectrum [15] is observed in the lower-wavenumber range [Fig. 4(b)]. Note that symmetric structures on k_y axis, dumbbell lobes, appear in the whole $\boldsymbol{k}$ space, as known from conjugate symmetry. The energy spectral peaks in the vicinity of $(k_x, k_y) = (0, \pm 14)$ correspond to the emergence of the zonal flow. This result is consistent with large energy dissipation observed in Ref. [24]. The energy spectrum has large values between the semicircle $|\boldsymbol{k}| \approx k_{\rm R}^\star$, and the dumbbell spectrum $k^8 \approx (k_\beta^\star)^5|k_x|^3$ with $k_{\rm R}^\star = k_\beta^\star = 14$.

To see the relation of this anisotropy to the energy flux, conventionally used 1D spectra and fluxes of energy and enstrophy are plotted in Figs. 4(c) and 4(d). In Fig. 4(c), anisotropy of the energy spectra is observed in low-wavenumber range, while isotropy as seen in Figs. 2(a) is in $|\boldsymbol{k}| \gtrsim 100$. Note that $E^{\rm yr}(k_x)$ and $E(k_x, 0)$ are sufficiently smooth, whereas $E^{\rm xr}(k_y)$ and $E(0, k_y)$ contain discrete peaks at harmonics of fundamental wavenumber $k_y = 14$, which suppress the nonlinear interaction of the Jacobian type. The energy spectrum tends to have an equilibrium spectrum $E^{\rm o}(k) = C\beta^2 k^{-5}$ owing to Rossby wave radiation [14,25]. Note that anisotropic wavenumber range varies depending on the types of the spectra; it starts roughly at 100 in on-axis spectrum, at 50 in unidirectionally reduced spectrum, and at 15 in 2D spectrum. As mentioned above, heterogeneous spectra are mixed by the omnidirectional ones at low wavenumbers and unidirectionally reduced ones at all wavenumbers.

Corresponding to the dumbbell spectrum, the energy fluxes shown in Fig. 4(d) demonstrate remarkable behavior in $|\boldsymbol{k}| \lesssim 15$: $P^{\rm yr}(k_x)$ remains negative and almost constant, while $P^{\rm xr}(k_y)$ and $P^{\rm o}(k)$ abruptly change to almost zero around k_y and $k = 14$, respectively. Small anisotropy in the high-wavenumber range becomes prominent because the vertical axis of Fig. 4(d) is set in linear scale, while that of Fig. 4(c) is in logarithmic scale. The anisotropy should decrease with increasing the inertial subranges. The enstrophy fluxes, $Q^{\rm o}(k)$, $Q^{\rm yr}(k_x)$ and $Q^{\rm xr}(k_y)$, remain nearly unaffected by the β effect, since their supports are in the high-wavenumber range. Because anisotropies in these fluxes are a mixture of different turbulence properties, local-flux vectors of conserved quantities are indispensable to reveal their roles in HCT.

The local-flux vectors of energy and enstrophy are shown in Fig. 5 as in Fig. 3. The global directional property of the local-flux vectors of energy shown in Fig. 5(a) is the same as the one in HIT [Fig. 3(a)], and consistent with the inverse energy cascade. The most remarkable difference appears in the low-wavenumber range [Fig. 5(b)] especially below the semicircle $|\boldsymbol{k}| \approx 14$. The directions of the inward vectors deviate from isotropic ones to surround the semicircle and outward direction from the origin in the dumbbell spectrum. The local-flux vectors indicate a new scenario that the narrow part of the dumbbell spectrum, the two lobes' point of tangency, is due to energy
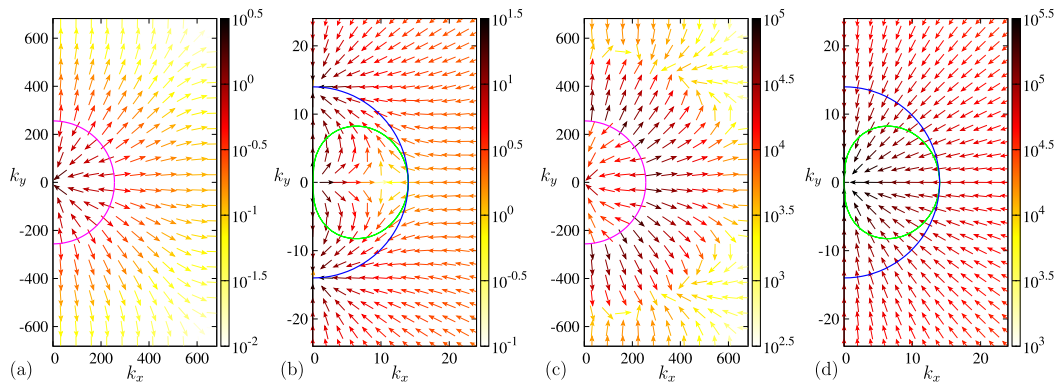
FIG. 5. In CHM turbulence, local-flux vectors of (a), (b) energy and (c), (d) enstrophy. See also the caption to Fig. 3.

accumulation along the k_y axis centered at $(k_x, k_y) \approx (0, \pm 14)$, where nonlinearity is suppressed to sustain the zonal flow. The local-flux vectors of enstrophy in Figs. 5(c) and 5(d) are almost the same as those of HIT in Figs. 3(c) and 3(d). Corresponding to the anisotropy observed in Fig. 4(d), $Q^{yr}(k_x)$ and $Q^{xr}(k_y)$, directional anisotropy is observed in Fig. 5(c) and becomes conspicuous in the small-flux region, $|\boldsymbol{k}| < k_f$ or $|\boldsymbol{k}| \gtrsim 600$, where the enstrophy flows inwardly. On the other hand, the enstrophy flows inwardly and almost isotropically in $|\boldsymbol{k}| \lesssim 14$, where local-flux vectors of energy show directional anisotropy.

In this Letter, we have proposed a simple method to uniquely determine flux vectors of conserved quantities in an anisotropic turbulence, which is a natural extension of conventionally used omnidirectional and unidirectionally reduced fluxes in HIT. The proposed local-flux vector is a special solution of the continuity equation (2), which connects the vector flux to a scalar transfer as its generalization in HIT, and is chosen for the vector flux to have a scalar potential.

We have applied the proposed method to the CHM turbulence as anisotropy-controlled study of 2D NS turbulence. The local-flux vectors successfully reveal the structures deduced from the cascade theory and critical balance in the whole $\boldsymbol{k}$ space and quantitatively evaluate the critical balance in HCT. The local-flux vectors show that the energy flows along the semicircle boundary obtained by term balancing rather than the dumbbell-shape boundary by time balancing, while enstrophy flows almost only in radial direction even in the dumbbell spectrum range. The local-flux vectors of energy also indicate the scenario to sustain the dumbbell spectrum. Care should be taken in investigating results from reduced spectra [Figs. 2(a) and 4(c)] and reduced fluxes [Figs. 2(b) and 4(d)] since they usually mix heterogeneous turbulence properties. Each of these spectra suggests different wavenumbers as a boundary of anisotropy.

Lastly, the proposed method will work well in general fields, regardless of its spatial dimension, statistically steadiness, spectral distribution, and so on. To reexamine the situation in Ref. [13] from a viewpoint of the local-flux vectors, the triple cascade and the generation of zonal flow will be investigated in a separate paper. Moreover, useful information would be obtained if the method is applied to anisotropic turbulence such as flows on a rotating sphere, magnetohydrodynamic turbulence, and wave turbulence subject to anisotropic initial and/or boundary conditions.

[1] J. G. Charney, Geostrophic turbulence, J. Atom. Sci. **28**, 1087 (1971); A. Hasegawa and K. Mima, Pseudo-three-dimensional turbulence in magnetized nonuniform plasma, Phys. Fluids **21**, 87 (1978); R. T. Pierrehumbert, I. M. Held, and K. L. Swanson, Spectra of local and nonlocal two-dimensional turbulence, Chaos Solitons Fractals **4**, 1111 (1994); T. Watanabe and T. Iwayama, Unified scaling theory for local and non-local transfers in generalized two-dimensional turbulence, J. Phys. Soc. Jpn **73**, 3319 (2004).

[2] A. Kolmogorov, The local structure of turbulence in incompressible viscous fluid for very large Reynolds numbers, Akademiia Nauk SSSR Doklady **30**, 301 (1941).

[3] R. Kraichnan, Inertial ranges in two-dimensional turbulence, Phys. Fluids **10**, 2080 (1967).

[4] R. Fjørtoft, On the changes in the spectral distribution of kinetic energy for two-dimensional non-divergent flow, Tellus **5**, 225 (1953).

[5] G. Boffetta and R. E. Ecke, Two-dimensional turbulence, Annu. Rev. Fluid Mech. **44**, 427 (2012); B. Burgess, R. Scott, and T. Shepherd, Kraichnan-Leith-Batchelor similarity theory and two-dimensional inverse cascades, J. Fluid Mech. **767**, 467 (2015).

[6] J. Jimenez, Dipoles and streams in two-dimensional turbulence, J. Fluid Mech. **904**, A39 (2020); I. V. Kolokolov and V. V. Lebedev, Coherent vortex in two-dimensional turbulence: Interplay of viscosity and bottom friction, Phys. Rev. E **102**, 023108 (2020).

[7] A. Alexakis and L. Biferale, Cascades and transitions in turbulent flows, Phys. Rep. **767–769**, 1 (2018).

[8] P. Goldreich and S. Sridhar, Toward a theory of interstellar turbulence. II. strong Alfvénic turbulence, Astrophys. J. **438**, 763 (1995); S. V. Nazarenko and A. A. Schekochihin, Critical balance in magnetohydrodynamic, rotating and stratified turbulence: towards a universal scaling conjecture, J. Fluid Mech. **677**, 134 (2011); R. Meyrand, S. Galtier, and K. H. Kiyani, Direct Evidence of the Transition from Weak to Strong Magnetohydrodynamic Turbulence, Phys. Rev. Lett. **116**, 105002 (2016).

[9] S. Nazarenko, *Wave Turbulence* (Springer, Heidelberg, 2011).

[10] F. Waleffe, The nature of triad interactions in homogeneous turbulence, Phys. Fluids A **4**, 350 (1992); K. Ohkitani and S. Kida, Triad interactions in a forced turbulence, *ibid.* **4**, 794 (1992).

[11] G. Dar, M. Verma, and V. Eswaran, Energy transfer in two-dimensional magnetohydrodynamic turbulence: formalism and numerical results, Physica D **157**, 207 (2001); S. Maeyama, M. Sasaki, K. Fujii, T. Kobayashi, R. Dendy, Y. Kawachi, H. Arakawa, and S. Inagaki, On the triad transfer analysis of plasma turbulence: symmetrization, coarse graining, and directional representation, New J. Phys. **23**, 043049 (2021); K. Obuse and M. Yamada, Energy transfer to resonant zonal Rossby modes in two-dimensional turbulence on a rotating sphere, J. Phys. Soc. Jpn. **89**, 064401 (2020).

[12] N. Yokoyama and M. Takaoka, Energy-flux vectors in anisotropic turbulence: Application to rotating turbulence, J. Fluid Mech. **908**, A17 (2021).

[13] S. Nazarenko and B. Quinn, Triple Cascade Behavior in Quasigeostrophic and Drift Turbulence and Generation of Zonal Jets, Phys. Rev. Lett. **103**, 118501 (2009).

[14] P. B. Rhines, Waves and turbulence on a beta-plane, J. Fluid Mech. **69**, 417 (1975).

[15] G. K. Vallis and M. E. Maltrud, Generation of mean flows and jets on a beta plane and over topography, J. Phys. Oceanogr. **23**, 1346 (1993).

[16] A. M. Balk, A new invariant for Rossby wave systems, Phys. Lett. A **155**, 20 (1991).

[17] W. H. Matthaeus, S. Oughton, and Y. Zhou, Anisotropic magnetohydrodynamic spectral transfer in the diffusion approximation, Phys. Rev. E **79**, 035401(R) (2009); S. Galtier and É. Buchlin, Nonlinear diffusion equations for anisotropic magnetohydrodynamic turbulence with cross-helicity, Astrophys. J. **722**, 1977 (2010).

[18] V. E. Zakharov, V. S. L'vov, and G. Falkovich, *Kolmogorov Spectra of Turbulence I* (Springer, Heidelberg, 1992).

[19] M. Yamada and T. Yoneda, Resonant interaction of Rossby waves in two-dimensional flow on a β plane, Physica D **245**, 1 (2013).

[20] E. Kartashova, *Nonlinear Resonance Analysis: Theory Computation, Applications* (Cambridge University Press, Cambridge, 2011).

[21] Z. Xiao, M. Wan, S. Chen, and G. Eyink, Physical mechanism of the inverse energy cascade of two-dimensional turbulence: a numerical investigation, J. Fluid Mech. **619**, 1 (2009); D. Qi and A. J.

Majda, Transient metastability and selective decay for the coherent zonal structures in plasma drift wave turbulence, J. Nonlinear Sci. **29**, 2297 (2019).

[22] P. Constantin, C. Foias, and O. Manley, Effects of the forcing function spectrum on energy spectrum in 2-d turbulence, Phys. Fluids **6**, 427 (1994); C. V. Tran and T. G. Shepherd, Constraints on the spectral distribution of energy and enstrophy dissipation in forced two-dimensional turbulence, Physica D **165**, 199 (2002).

[23] G. Boffetta, Energy and enstrophy fluxes in the double cascade of two-dimensional turbulence, J. Fluid Mech. **589**, 253 (2007); G. Boffetta and S. Musacchio, Evidence for the double cascade scenario in two-dimensional turbulence, Phys. Rev. E **82**, 016307 (2010).

[24] S. Sukoriansky, N. Dikovskaya, and B. Galperin, On the arrest of inverse energy cascade and the Rhines scale, J. Atom. Sci. **64**, 3312 (2007).

[25] B. Galperin, S. Sukoriansky, and H.-P. Huang, Universal n^{-5} spectrum of zonal flows on giant planets, Phys. Fluids **13**, 1545 (2001).